Dual-Wavelength Y-Branch DBR Lasers With 100 mW of CW Power Near 2 μm

Jiang Jiang, Leon Shterengas, Aaron Stein, Gela Kipshidze, *Member, IEEE*, Alexey Belyanin, and Gregory Belenky, *Fellow, IEEE*

***Abstract*— The interband GaSb-based diode lasers emitting simultaneously in two narrow bands separated by either ∼1.6 or ∼3.3 THz were designed, fabricated and characterized. The device active region contained one asymmetric tunnel-coupled double quantum well with separation between two lowest electron subbands controlled by thickness of the tunnel barrier. The Y-branch 6th order distributed Bragg reflector devices have been fabricated with either deep or shallow etched ridge waveguides. The increase of the deeply etched ridge waveguide width from 10 to 20 μm improved laser threshold and efficiency thanks to reduction of the relative role of the sidewall defect recombination. Further improvement of the device performance parameter was achieved by shallow etching. The shallow etched lasers with stable dual-wavelength emission spectrum generated 100 mW of continuous wave output power at 20 °C.**

***Index Terms*— Mid-infrared, Y-branch, DBR, type-I quantum well, GaSb-based, semiconductor lasers.**

I. Introduction

THE high power dual-wavelength GaSb-based lasers operating above 2 μm are required for development of the new class of compact, room temperature operated THz emitters either based on intra-cavity difference frequency generation [1], [2] or utilizing external antenna-based photo mixers [3], [4]. The development of the corresponding converters operating near 2 μm is still at the early stage, but they can promise reduction of the threshold power leading to significantly simplified system design for continuous wave (CW) intra-cavity THz generation. We have reported on the first generation of GaSb-based dual-wavelength emitters operating near 2.1 μm in reference [5]. The design concept was closely following the Y-branch distributed Bragg reflector (DBR) architecture used for development of the dual-wavelength near-infrared emitters based on GaAs material system [6], [7]. The first generation of the GaSb-based dual-wavelength lasers utilized 10-μm-wide deeply etched ridge waveguides and demonstrated the CW output power of ∼10 mW at heatsink temperature of ∼2 °C. In this work we report on the second generation of the GaSb-based dual-wavelength lasers with significantly improved operating parameters. The roles of the etching depth and width of the ridge waveguide were investigated experimentally. We have reduced the number of the asymmetric tunnel-coupled quantum wells (QW) in active region and optimized the periods of the DBR reflectors to improve the stability of the laser dual band emission spectra. The dual-wavelength operation with CW output power above 100 mW at 20 °C accompanied by nearly fourfold reduction of the laser threshold current was demonstrated in shallow ridge waveguide Y-branch 6th order DBR lasers. The lasers emitted in two narrow bands separated by either ∼1.6 or ∼3.3 THz in the whole range of the operating currents near and above room temperature.

II. Device Fabrication

Laser heterostructures were grown by solid source molecular beam epitaxy on tellurium doped n-GaSb substrates. The 2-μm-thick n- and 1.5-μm-thick p-claddings were made of Te- and Be-doped $Al_{0.6}Ga_{0.4}As_{0.05}Sb_{0.95}$ alloys. The 400-nm-thick nominally undoped waveguide core contained one asymmetric tunnel-coupled double QW (Figure 1a) in its center. The QW contained three layers (from left to right): $Ga_{0.75}In_{0.25}Sb$, $Al_{0.2}Ga_{0.8}As_{0.02}Sb_{0.98}$ tunnel barrier, and $Ga_{0.92}In_{0.08}As_{0.07}Sb_{0.93}$. The design of the tunnel-coupled asymmetric QWs with theoretically predicted strong resonant second order nonlinearity was described in detail in [5], [8]. In this work we studied devices containing two types of the QWs with tunnel barriers of nominal thicknesses of either 2 nm in structure H1 or 3 nm in structure H2. The increase of the tunnel barrier thickness resulted into reduced separation between e1 and e2 electron subbands in active QW of structure H2. The structure H1 used $Al_{0.2}Ga_{0.8}As_{0.02}Sb_{0.98}$ waveguide core material while the structure H2 used $Al_{0.3}Ga_{0.7}As_{0.03}Sb_{0.97}$ to improve QW

Manuscript received April 26, 2020; revised July 9, 2020; accepted July 11, 2020. Date of publication July 16, 2020; date of current version July 27, 2020. This work was supported in part by the U.S. National Science Foundation under Grant ECCS-1707317US and in part by the U.S. Department of Energy, Office of Basic Energy Sciences, through the Center for Functional Nanomaterials, Brookhaven National Laboratory, under Contract DE-SC0012704. *(Corresponding author: Jiang Jiang.)*

Jiang Jiang, Leon Shterengas, Gela Kipshidze, and Gregory Belenky are with the Department of Electrical and Computer Engineering, State University of New York at Stony Brook, Stony Brook, NY 11794 USA (e-mail: jiang.jiang@stonybrook.edu; leon.shterengas@stonybrook.edu).

Aaron Stein is with the Center for Functional Nanomaterials, Brookhaven National Laboratory, Upton, NY 11973 USA.

Alexey Belyanin is with the Department of Physics and Astronomy, Texas A&M University at College Station, College Station, TX 77843 USA.

Color versions of one or more of the figures in this letter are available online at http://ieeexplore.ieee.org.

Digital Object Identifier 10.1109/LPT.2020.3009663

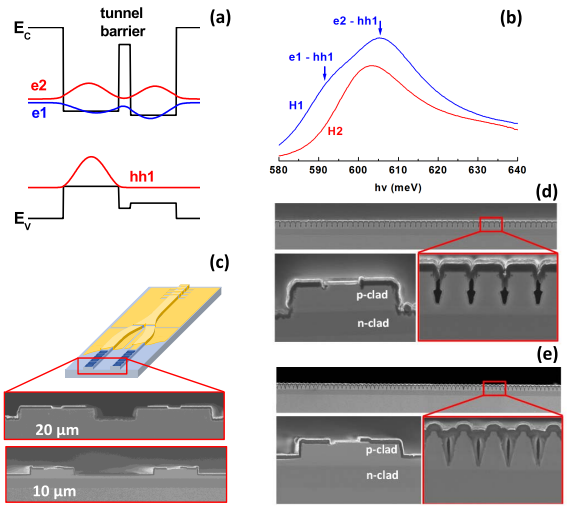

Fig. 1. (a) Band edges and envelope wavefunctions of the e1, e2 and hh1 states of the asymmetric tunnel-coupled double QW; (b) Room temperature PL spectra of the H1 an H2 laser heterostructures – the approximate energies of the e1-hh1 and e2-hh1 transitions are shown by arrows for H1 structure; (c) The illustration of the design of the Y-branch DBR lasers and cross-section scanning electron microscope (SEM) images of the cleaved two-ridge section with 20- and 10-μm-wide ridge waveguides; (d) and (e) - SEM images illustrating ridge and DBR etching profiles in the deeply etched H1 and shallow etched H2 structures, respectively.

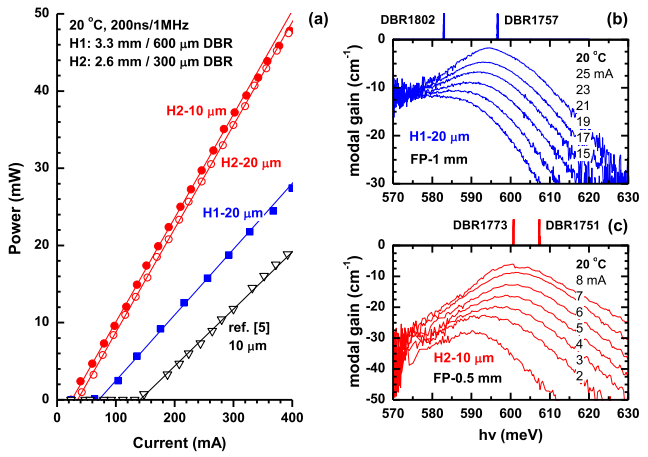

Fig. 2. (a) Power-current characteristics of uncoated DBR lasers based on structures H1 and H2. The 20-μm-wide deeply etched ridges of the DBR lasers based on structure H1 had total length of 3.3 mm with 600-μm-long DBR section. The 10- and 20-μm-wide shallow etched ridge DBR lasers based on structure H2 had total length of 2.6 mm with ~300-μm-long DBR section. The data from ref. [5] for 10-μm-wide deeply etched 3.3-mm-long devices with 600 μm DBR section is shown for reference. (b) and (c) - The modal gain spectra of the FP lasers based on H1 structure and having cavity length of 1 mm and ridge width of 20 μm (b); and on H2 structure having cavity length of 0.5 mm and ridge width of 10 μm (c). The corresponding emission spectra of the DBR lasers of different grating periods are shown above the gain curves.

carrier confinement. Room temperature photoluminescence (PL) spectra confirmed the reduced energy separation between e1-hh1 and e2-hh1 optical transitions in H2 structures compared to that of H1 (Figure 1b) as well as that of structure used in reference [5]. The PL peaks corresponding to e1-hh1 and e2-hh1 optical transitions are separated by ~15 meV in H1 and thus can be well resolved in room temperature PL spectra. The increase of the tunnel barrier thickness to 3 nm, as expected, reduced the energy separation between e1-hh1 and e2-hh1 transition down to below 10 meV and the corresponding PL peaks merged together (Figure 1b).

Both wafers were processed into Y-branch 6th order DBR lasers with up to 1.3-mm-long two-ridge section with ridge center-to-center spacing of 30 μm, 1-mm-long Y-branch transition section and up to 1-mm-long single ridge section (Figure 1c). The DBR reflectors terminated the two-ridge section facets.

We fabricated devices with 10- and 20-μm-wide ridges using silicon nitride hard mask and chlorine-based inductively coupled plasma reactive ion etching (ICP-RIE). The structure H1 was fabricated using simplified process relying on single hard mask containing features defining both ridges and DBR gratings. The etching depth in the DBR section was controlled to stop at the interface between p-cladding and waveguide core (Figure 1d) to ensure strong coupling of the laser mode to DBR grating [9]. Due to higher etching rate in the large open area (compared to the ~200-nm-wide openings in hard mask in grating section) the ridges were etched down to n-cladding (Figure 1d). The etching through active region resulted into excessive sidewall recombination controlling carrier lifetime in narrower ridges and leading to increased threshold current density as discussed further in the text. The structure H2 was etched in two steps using two separately fabricated hard masks. The DBR gratings were etched using the first hard mask utilizing the dry etching chemistry specifically optimized for V-shape high aspect ratio etching (Figure 1e). The shallow ridges were formed afterwards in the separate etching run using second hard mask and utilizing dry etch chemistry optimized for smooth etched surface morphology. The second process applied to structure H2 was more labor intensive but allowed for independent control over etching depths in DBR grating and ridge sections. As a result, the devices based on structure H2 had superior etching profiles (Figure 1e) compared to devices based on structure H1 leading to superior laser performance parameters. The DBR grating with periods 1757 and 1802 nm (DBR1757 and DBR1802) were used in structure H1 while the structure H2 utilized DBRs with periods of 1751 and 1773 nm (DBR1751 and DBR1773). The reference straight ridge DBR lasers have been fabricated next to the Y-branch DBR lasers. We also cleaved the Fabry-Perot (FP) devices without DBR gratings from the same wafers for optical gain and loss measurements.

III. Device Characterization and Discussion

The fabricated single ridge narrow spectrum DBR and dual-wavelength Y-branch DBR lasers demonstrated significant improvement of the operating parameters compared to the first generation of the devices reported in [5]. Figure 2a plots the power-current characteristics of the straight ridge single DBR lasers. The 20-μm-wide deeply etched ridge devices based on H1 heterostructure demonstrated nearly twofold reduction of the threshold current compared to 10-μm-wide deeply etched ridge lasers reported in [5]. The 10-μm-wide ridges based on H1 (not shown) also demonstrate higher threshold

(~100 mA) compared to H1 20-μm-wide devices. Arguably, the reduction of the threshold current with increasing ridge width can be explained by decreasing contribution of the nonradiative recombination and scattering rates at the etched ridge sidewalls.

The Figure 2b plots the modal gain spectra measured by Hakki-Paoli method [10] at several currents below threshold for 1-mm-long 20-μm-wide uncoated FP H1 lasers. The device transparency current density can be estimated as ~75 A/cm^2. The internal optical loss of ~2 cm^{-1} were estimated for H1 FP lasers by both direct modal gain measurements and variable cavity technique (not shown). The laser internal efficiency was ~65%. The measurement of the slope efficiency of the DBR lasers allows for rough estimation of the extra equivalent distributed optical loss associated with the 6th order DBR grating as about 4 cm^{-1}. This requires threshold gain of about 8 cm^{-1} corresponding to the pumping current of about 23 mA for 1-mm-long FP devices which roughly corresponds to ~70 mA threshold observed in 3.3-mm-long DBR lasers. The positions of the DBR-controlled emission lines are shown in the top part of the picture. The line separation was to match PL peak separation (Figure 1b). The increase of the laser temperature above 20 °C would be beneficial to obtain similar gains at both DBR lines in dual-wavelength Y-branch devices.

The use of shallow etching in H2 devices further improved the laser threshold thanks to elimination of the surface recombination issue at the ridge sidewalls - the etching stopped in top p-cladding. Hence, the reduction of the ridge waveguide width from 20 to 10 μm in DBR H2 lasers further decreased the threshold down to about 25 mA. The minimization of the side wall scattering and improvement of the internal efficiency due to stronger carrier confinement in active QW helped to increase the H2 DBR laser slope efficiency. The relative position of the DBR controlled emission lines and the gain peak for H2 lasers is illustrated in Figure 2c. The DBR laser lines separation was designed to match the energy spacing between e1-hh1 and e2-hh1 transitions of H2 laser heterostructure based on QW with ~3-nm-wide tunnel barrier (Figure 1b). The gain spectra measured for 0.5-mm-long 10-μm-wide FP lasers (Figure 2c) were distorted for energies below 585 meV due to incomplete filtering of the higher-order lateral modes but the transparency current density below ~50 A/cm^2 could still be estimated. It is expected that H2 devices should have similar internal losses to that of H1 lasers. The threshold gain for 2.6-mm-long 10-μm-wide DBR lasers corresponds to the gain curve measured at ~5 mA for 0.5-mm-long FP devices (Figure 2c). It should be noted that all DBR devices studied in this work generated narrow, DBR grating-controlled emission spectra in the whole range of the operating currents in contrast to FP lasers which emitted usual wide band multimode spectra.

The Y-branch DBR lasers based on structure H1 operated in stable dual-wavelength regime at temperatures above 30 °C. The Figure 3 plots power-current characteristics of the Y-branch DBR H1 lasers measured in pulsed (200ns/1MHz) regime at 20 °C and 40 °C as well as power-current-voltage characteristics measured in CW regime at 30 °C. The threshold current of the Y-branch lasers is about 120 mA

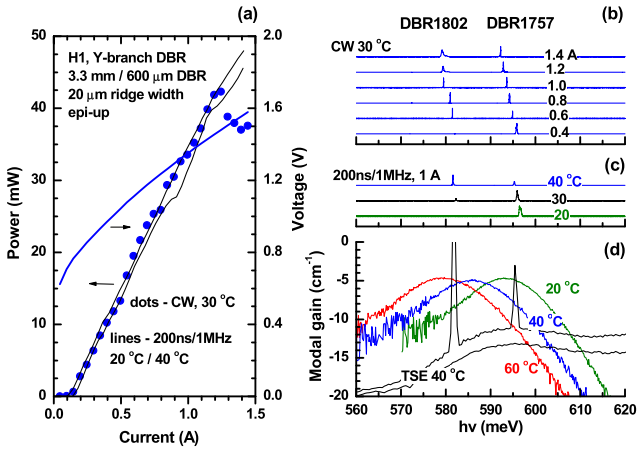

Fig. 3. (a) Power-current-voltage characteristics of the uncoated 20 μm ridge Y-branch DBR H1 lasers. Devices have the length of 3.3 mm with 600-μm-long DBR sections; (b) The current dependence of the CW laser emission spectra at 30 °C; (c) The pulsed laser emission at 20, 30 and 40 °C at 1A; (d) Modal gain spectra of 1-mm-long 20-μm-wide FP H1 lasers at 20 °C (23 mA), 40 °C (27 mA) and 60 °C (34mA). The 40 °C (200ns/100kHz) true spontaneous emission spectra measured below (100mA) and above (250 mA) threshold are also shown.

which is ~1.6 times higher than that of single DBR lasers of the same length (Figure 2a) as expected for devices with ~1.6 larger ridge area. The slope efficiency of the Y-branch lasers was reduced compared to that of straight ridge DBR lasers due to sharing of the gain in single ridge section and extra scattering loss expected in Y-branch section. In pulsed regime at 20 °C the Y-branch lasers emit only at DBR1757-controlled wavelength because of detuning of the gain peak from the DBR1802 line (Figure 3c and 3d). Increase of the laser temperature to 30 °C improved alignment between gain peak and DBR1802 line and both DBR-controlled lasing lines contributed to emission spectrum (Figure 3c). Further increase of the laser temperature to 40 °C favors lasing at DBR1802 line. In CW regime the stable dual-wavelength operation with comparable intensities of the both DBR-controlled laser lines was observed at heatsink temperature of 30 °C (the actual laser temperature in CW regime is higher than heatsink temperature). The maximum CW output power is above 40 mW in dual-wavelength regime corresponding to the DBR line separation of about 3.3 THz.

The Y-branch DBR lasers based on structure H2 also demonstrate scaling of the threshold and efficiency roughly proportional to the increase of the ridge waveguide footprint. Similarly, to the single DBR lasers the power-current-voltage characteristics of the shallow etched Y-branch DBR H2 lasers are close to each other for 10- and 20-μm-wide ridge devices (Figure 4a). Both types of lasers operated in stable dual-wavelength regime at 20 °C thanks to the good alignment of both DBR-controlled lines to the gain peak. Figure 4b shows the current dependence of the CW emission spectrum of the 10-μm-wide Y-branch DBR H2 lasers at 20 °C. The smaller separation between DBR laser lines corresponding to ~1.6 THz also helps to stabilize the dual wavelength operation. The devices generated in excess of 100 mW CW output power (about 5 MW/cm^2 of intracavity power density)

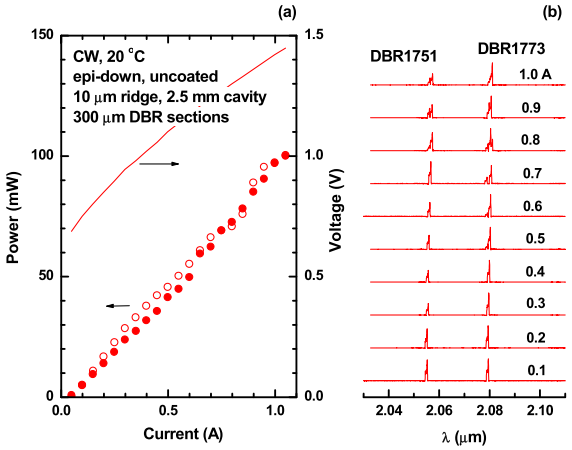

Fig. 4. (a) Power-current-voltage characteristics of the uncoated Y-branch DBR H2 lasers with 10-μm-wide (solid circles) and 20-μm-wide (open circles) ridge waveguides. Device lengths are 2.5 mm with 300 μm-long DBR sections; (b) The CW current dependence of the 10 μm ridge laser emission spectra at 20 °C.

at 1 A in dual-wavelength regime near 2.07 μm. The Joule heat generated at this current is just below 1.5 W which can easily be handled by standard small-size thermo-electrical coolers. For the intra-cavity difference frequency generation utilizing theoretically predicted resonant second order nonlinearity of the active tunnel-coupled asymmetric double QW, the 10-μm-wide ridge devices are preferred thanks to increased intracavity intensity of the $\lambda \sim 2$ μm pump radiation.

The Cherenkov outcoupling scheme [1] of the anticipated THz radiation is not an efficient solution for lasers grown on conducting GaSb substrates. Metamorphic growth on semi-isolating substrates [11] can open this possibility. Alternatively, the intra-cavity generated THz current sheet can radiate directly into the vacuum electromagnetic modes through interaction with the surface grating. The corresponding THz output power (P_{THz}) can be estimated as (the formula is in CGS units):

$$P_{THz} \sim 128\pi^5 \eta_{grat} \frac{L_{cav}}{L_{lat}} \frac{w_{nl}^2}{w_{opt}^2} \frac{\left|\chi^{(2)}\right|^2}{\lambda_{THz}^2 cn} P_1 P_2.$$

For the cavity length $L_{cav} \sim 1$ mm; the lateral and vertical widths of the laser mode $L_{lat} \sim 10$ μm and $w_{opt} \sim 0.5$ μm, respectively; the effective width of the nonlinear current layer $w_{nl} \sim 20$ nm; $\lambda_{\mathrm{THz}} \sim 100$ μm; the second order nonlinear susceptibility $\chi^{(2)} \sim 0.0025$ esu [8]; refractive index $n \sim 3.5$ and grating outcoupling efficiency $\eta_{grat} \sim 1\%$, the THz generation efficiency of $\sim$0.0004 W/W^2 can be estimated. Therefore, μW level THz output power seem to be feasible even for the current devices. Surface grating outcoupling can also be arranged in double metal waveguide structures [12] which are compatible with antimonide technology.

IV. Conclusion

The effect of the ridge waveguide parameters on threshold current and output power of the $\lambda \sim 2.1$ μm Y-branch DBR dual-wavelength GaSb-based diode lasers was studied. The devices with shallow etched ridges demonstrated 100 mW output power with emission spectrum in two narrow bands separated by $\sim$1.6 THz at 20 °C. The shallow etched DBR lasers with 10 and 20 μm ridge waveguides demonstrated the same efficiencies and output power levels but threshold currents were reduced in narrower ridges. For deeply etched lasers both the threshold and efficiency improved when ridge width was increased from 10 to 20 μm. The deeply etched lasers with 20-μm ridges demonstrated in excess of 40 mW of output power at 30 °C and emitted at two narrow bands separated by $\sim$3.3 THz. The active region of the lasers contained an asymmetric tunnel-coupled double QW with theoretically predicted strong resonant second-order nonlinearity. The devices reported in this work demonstrated order of magnitude improvement of the output power and multifold improvement of the threshold current compared to the first generation of the GaSb-based dual-wavelength Y-branch DBR lasers. It is also important that the devices generated comparable power at the two wavelengths over a broad range of currents, since the power of the difference-frequency signal is proportional to the product of the two pump powers. The lasers required below 1.5 W of the electrical power at maximum CW output power level and can be utilized for efficient intra-cavity or extra-cavity difference frequency generation of the THz radiation.

References

[1] K. Fujita *et al.*, "Recent progress in terahertz difference-frequency quantum cascade laser sources," *Nanophotonics*, vol. 7, no. 11, pp. 1795–1817, Sep. 2018.
[2] Q. Lu, F. Wang, D. Wu, S. Slivken, and M. Razeghi, "Room temperature terahertz semiconductor frequency comb," *Nature Commun.*, vol. 10, no. 1, p. 2403, Jun. 2019.
[3] S. Preu, G. H. Döhler, S. Malzer, L. J. Wang, and A. C. Gossard, "Tunable, continuous-wave terahertz photomixer sources and applications," *J. Appl. Phys.*, vol. 109, no. 6, Mar. 2011, Art. no. 061301.
[4] J. O. Gwaro, C. Brenner, L. S. Theurer, M. Maiwald, B. Sumpf, and M. R. Hofmann, "Continuous wave THz system based on an electrically tunable monolithic dual wavelength Y-branch DBR diode laser," *J. Infr., Millim., Terahertz Waves*, vol. 41, no. 5, pp. 568–575, May 2020.
[5] J. Jiang *et al.*, "Dual wavelength operation of the GaSb-based Y-branch distributed Bragg reflector lasers near 2.1 μm," *Semicond. Sci. Technol.*, vol. 35, no. 2, Jan. 2020, Art. no. 025016.
[6] B. Sumpf *et al.*, "Dual-wavelength diode laser with electrically adjustable wavelength distance at 785 nm," *Opt. Lett.*, vol. 41, no. 16, pp. 3694–3697, Aug. 2016.
[7] B. Sumpf *et al.*, "Comparison of two concepts for dual-wavelength DBR ridge waveguide diode lasers at 785 nm suitable for shifted excitation Raman difference spectroscopy," *Appl. Phys. B, Lasers Opt.*, vol. 120, no. 2, pp. 261–269, May 2015.
[8] J. Jiang, L. Shterengas, T. Hosoda, A. Belyanin, G. Kipshidze, and G. Belenky, "GaSb-based diode lasers with asymmetric coupled quantum wells," *Appl. Phys. Lett.*, vol. 113, no. 7, Aug. 2018, Art. no. 071106.
[9] J. Fricke *et al.*, "Properties and fabrication of high-order Bragg gratings for wavelength stabilization of diode lasers," *Semicond. Sci. Technol.*, vol. 27, no. 5, Apr. 2012, Art. no. 055009.
[10] B. W. Hakki and T. L. Paoli, "Gain spectra in GaAs double- heterostructure injection lasers," *J. Appl. Phys.*, vol. 46, no. 3, pp. 1299–1306, Mar. 1975.
[11] C. J. K. Richardson, L. He, P. Apiratikul, N. P. Siwak, and R. P. Leavitt, "Improved GaSb-based quantum well laser performance through metamorphic growth on GaAs substrates," *Appl. Phys. Lett.*, vol. 106, no. 10, Mar. 2015, Art. no. 101108.
[12] C. Pflügl *et al.*, "Surface-emitting terahertz quantum cascade laser source based on intracavity difference-frequency generation," *Appl. Phys. Lett.*, vol. 93, no. 16, Oct. 2008, Art. no. 161110.